JCTC Journal of Chemical Theory and Computation

Article

pubs.acs.org/JCTC

Exploring the Light-Capturing Properties of Photosynthetic Chlorophyll Clusters Using Large-Scale Correlated Calculations

Carl-Mikael Suomivuori,[†,‡] Nina O. C. Winter,[§] Christof Hättig,[§] Dage Sundholm,[†] and Ville R. I. Kaila*[,‡]

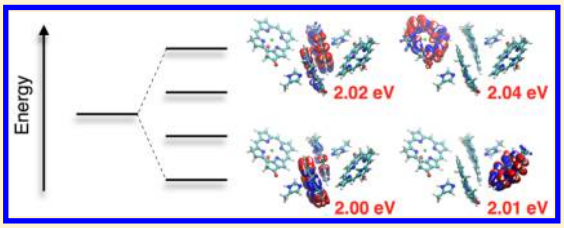
[†]Department of Chemistry, University of Helsinki, P.O. Box 55 (A. I. Virtanens plats 1), FIN-00014 Helsinki, Finland

[‡]Department Chemie, Technische Universität München, Lichtenbergstraße 4, Garching, Germany

[§]Ruhr-University at Bochum, Universitätsstraße 150, 44801 Bochum, Germany

Supporting Information

ABSTRACT: Chlorophylls are light-capturing units found in photosynthetic proteins. We study here the ground and excited state properties of monomeric, dimeric, and tetrameric models of the special chlorophyll/bacteriochlorophyll (Chl/BChl) pigment (P) centers P700 and P680/P870 of type I and type II photosystems, respectively. In the excited state calculations, we study the performance of the algebraic diagrammatic construction through second-order (ADC(2)) method in combination with the reduced virtual space (RVS) approach and the recently developed Laplace-transformed scaled-opposite-spin (LT-SOS) algorithm, which allows us, for the first time, to address multimeric effects at correlated *ab initio* levels using large basis sets. At the LT-SOS-RVS-ADC(2)/def2-TZVP level, we obtain vertical excitation energies (VEEs) of 2.00−2.07 and 1.52−1.62 eV for the P680/P700 and the P870 pigment models, respectively, which agree well with the experimental absorption maxima of 1.82, 1.77, and 1.43 eV for P680, P700, and P870, respectively. In the P680/P870 models, we find that the photoexcitation leads to a $\pi \rightarrow \pi^*$ transition in which the exciton is delocalized between the adjacent Chl/BChl molecules of the central pair, whereas the exciton is localized to a single chlorophyll molecule in the P700 model. Consistent with experiments, the calculated excitonic splittings between the central pairs of P680, P700, and P870 models are 80, 200, and 400 cm^{-1}, respectively. The calculations show that the electron affinity of the radical cation of the P680 model is 0.4 V larger than for the P870 model and 0.2 V larger than for P700. The chromophore stacking interaction is found to strongly influence the electron localization properties of the light-absorbing pigments, which may help to elucidate mechanistic details of the charge separation process in type I and type II photosystems.



INTRODUCTION

Photosynthesis is the primary biological energy conversion process, in which the energy of sunlight is converted into chemical energy.[1,2] Photosystem II (PSII) of green plants and cyanobacteria catalyzes this process by converting light energy into a flux of protons and electrons, which is used for reduction of quinones (Q) and oxidation of water. The oxidized water forms molecular oxygen, which in turn powers the respiratory chains of all aerobic organisms.[3]

The photosynthetic type I and type II reaction centers comprise a central chlorophyll (Chl) or bacteriochlorophyll (BChl) pigment cluster,[4−7] shown in Figure 1, that functions as the primary site for light capture and charge separation, which in turn provides the thermodynamic driving force for the Q reduction. The Chl/BChl clusters are often referred to as special pigment (P) pairs: P680 in PSII, P700 in photosystem I (PSI), and P870 in the photosynthetic bacterial reaction center (RC), after their respective absorption peaks at 680, 700, and 870 nm. Photoexcitation of this chlorophyll cluster leads to a charge separation process on a picosecond time scale, in which the electron is transferred to Q via an accessory pheophytin (Ph, Figure 1).[8−11] This results in the formation of a cationic $P^{+/\bullet}$ state, which is re-reduced by extracting electrons, either from water molecules in PSII by the catalytic manganese−calcium center (Mn_4O_5Ca) or by using an external electron donor protein as in the RC of purple bacteria and in PSI (Figure 1). The cationic $P680^{+/\bullet}$ in PSII has an unusually high oxidation potential of 1.2−1.4 V,[12] which is 0.5−0.9 V higher than for isolated chlorophylls in organic solvents and for the RC of purple bacteria.[13,14] The large redox shift has been suggested to arise from differences in the chromophore stacking, localization of the cationic charge, intrinsic differences between chlorophylls and bacteriochlorophylls, and electrostatic differences in the local protein environment.[1,15−20]

In this study, we aim at elucidating intrinsic differences in the electronic structures of the ground and excited states of the Chl and BChl pigments of PSI/PSII and of the bacterial RC using large-scale quantum chemical correlated *ab initio* and density functional theory (DFT) calculations. In the *ab initio* algebraic diagrammatic construction through second-order (ADC(2)) calculations, we utilize the recently implemented Laplace-transformed (LT) scaled-opposite-spin (SOS) approach in combination with the reduced virtual space (RVS) approximation,[21−25] allowing us to address multimeric effects at *ab initio* correlated levels of theory for the first time.

Received: March 2, 2016
Published: May 6, 2016

ACS Publications © 2016 American Chemical Society

DOI: 10.1021/acs.jctc.6b00237
J. Chem. Theory Comput. 2016, 12, 2644−2651

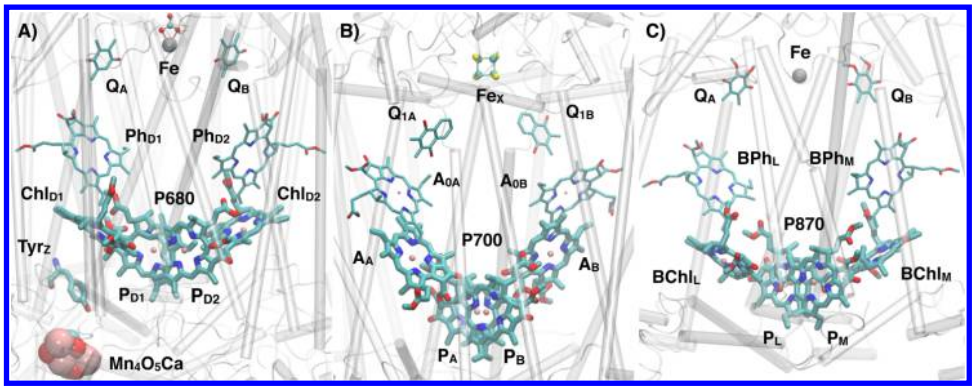


Figure 1. Structures of the photoactive centers in (A) PSII from *Thermosynechococcus vulcanus* (PDB ID: 3ARC), (B) PSI from *Synechoccus elongantus* (PDB ID: 1JB0), and (C) P870 from *Rhodobacter sphaeroides* (PDB ID: 3I4D).

METHODS

Molecular Structures. The Chl/BChl cluster models of P680, P700, and P870 were constructed based on the X-ray structures of *Thermosynechococcus vulcanus* (PDB ID: 3ARC),[4] *Synechoccus elongantus* (PDB ID: 1JB0),[5] and *Rhodobacter sphaeroides* (PDB ID: 3I4D),[6] obtained from the Protein Data Bank. The models consist of monomeric (54−88 atoms), dimeric (84−112 atoms), and tetrameric (198−224 atoms) Chl and BChl clusters with and without ligating histidine residues and water molecules. In the following, the presence of a ligand is denoted Chl/BChl-L. The chlorin and bacteriochlorin substituents were replaced by hydrogens in all models except for the monomer models, for which we also optimized a model with all substituents except for the long phytyl side chain. The phytyl chain was omitted due to its small effect on the excitation energy.[26] The terminal carbon atoms of the histidines and on the BChl and Chl rings were fixed in the optimization to consider the effect of the protein strain imposed by the different photosystems.

Ground State Calculations. The Chl/BChl model systems were optimized at the density functional theory (DFT) level using Becke's three parameter hybrid functional (B3LYP)[27,28] combined with Grimme's dispersion correction (B3LYP-D3)[29] and the Karlsruhe split valence polarization basis sets (def2-SVP).[30,31] The dielectric polarization of the protein environment was modeled using the conductor-like screening (COSMO) model[32,33] with the dielectric constant set to 4. The molecular structures of the models were optimized for both the neutral (P) and the cationic ($P^{+/\bullet}$) forms of the Chl/BChl clusters. The oxidation potentials relative to the normal hydrogen electrode (NHE of 4.43 eV) were obtained by calculating single-point energies for the optimized P and $P^{+/\bullet}$ forms at the B3LYP-D3 level using the Karlsruhe triple-ζ polarization basis sets (def2-TZVP).[27−29,31] Ground state energies and spin distributions of the cationic model systems were obtained from single-point calculations at the B3LYP-D3/def2-TZVP/COSMO level.

Excited State Calculations. Vertical excitation energies (VEEs) were calculated for the P680, P700, and P870 models at the algebraic diagrammatic construction through second-order (ADC(2)) level using the resolution-of-the-identity (RI) approximation and the Laplace-transformed (LT) scaled-opposite-spin (SOS) approach in combination with the reduced virtual space (RVS) approximation using a cutoff threshold of 50 eV above the highest occupied molecular orbital (RVS50).[21−25,34−38] In the excited state calculations, the def2-TZVP basis sets were used.[30,31] The basis set convergence is shown in Table 1 of the Supporting Information. Excitation energies for the Chl and BChl monomers were also obtained in calculations at the second-order approximate coupled-cluster (CC2) level. The calculations were performed using developer versions 6.3.1 and 6.6 of TURBOMOLE.[39,40]

Laplace Transformation. The coupled-cluster approximate singles and doubles (CC2)[41] method and related computational levels, such as the doubles correction to configuration interaction singles (CIS(D))[42] and ADC(2)[34] methods, scale formally a N^5, where N is the size of the basis set.[38,43] The computational costs for the SOS ansatz of these low-order *ab initio* correlation methods can be reduced to scale as N^4 when employing the RI approximation for the two-electron integrals and reformulating the most time-consuming step using a Laplace transformation,[21,22] the integral of which is calculated numerically using quadrature. The SOS-CC2 family of methods has been found to yield excitation energies with an accuracy comparable to the corresponding unscaled methods.[23,44] Comparison of 76 singlet states with more than 80% T_1 character reported by Schreiber et al.[45] shows that the mean average deviation (MAD) between the excitation energies calculated at the unscaled CC2 and the approximate singles, doubles, and triples (CC3)[46] levels is 0.097 eV, while the maximum deviation is 0.27 eV. We have considered only those states for which a best estimate is reported. Benchmarking of excitation energies calculated at the ADC(2) level yielded a similar accuracy as obtained at the unscaled CC2 level.[44] Moreover, a recent benchmarking study on the performance of scaled and unscaled CC2 and ADC(2) for excited state structures was recently presented by Tuna et al.[47]

The time-determining step for SOS-ADC(2), as for SOS-CC2, is the calculation of the intermediate

$$Y_{ai}^{Q} = c_{os} \sum_{bj} t_{ij}^{ab} B_{bj}^{Q} \tag{1}$$

where $c_{os} = 1.3$ is the SOS coefficient, and B_{pq}^{P} is the three-index intermediate obtained from the RI approximation of the four-index electron repulsion integrals.[23] In the RI approximation, the doubles amplitudes (t_{ij}^{ab}) of the CC2 family of methods are given by

$$t_{ij}^{ab} = -\frac{\sum_P B_{ai}^{P}, B_{bj}^{P}}{\epsilon_{iajb}} \tag{2}$$

DOI: 10.1021/acs.jctc.6b00237
J. Chem. Theory Comput. 2016, 12, 2644−2651

where ϵ_{iajb} is the difference between orbital energies.[21−24,36,37,48−50] The numerical approximation of the Laplace transformation of the energy denominator yields

$$\frac{1}{\epsilon_{iajb}} = \int_0^\infty \exp(-\epsilon_{iajb}t)dt \approx \sum_z^{n_L} w_z \exp(-\epsilon_{iajb}t_z) = \sum_z^{n_L} w_z \exp(-\epsilon_{ia}t_z)\exp(-\epsilon_{jb}t_z) \quad (3)$$

where $\epsilon_{ia} = \epsilon_i - \epsilon_a$ and $\epsilon_{jb} = \epsilon_j - \epsilon_b$ are the differences between the orbital energies of the occupied molecular orbitals i and j and the unoccupied a and b orbitals, respectively, w_z is the weight of the numerical integration scheme, and t_z is the corresponding integration point. In this approximation, t_{ij}^{ab} is given by

$$t_{ij}^{ab} = -\sum_z^{n_L} w_z \sum_P B_{ai}^P \exp(-\epsilon_{ai}t_z) B_{bj}^P \exp(-\epsilon_{bj}t_z) \quad (4)$$

and the most time-consuming intermediate can then be expressed as

$$Y_{ai}^Q = -c_{os} \sum_z^{n_L} w_z \sum_P N_z^{PQ} B_{ai}^P \exp(-\epsilon_{ai}t_z) \quad (5)$$

with

$$N_z^{PQ} = \sum_{bj} B_{bj}^Q B_{bj}^P \exp(-\epsilon_{bj}t_z) \quad (6)$$

where $n_L = 3-4$ is the number of integrations points for the Chl and BChl models, respectively, which yields a precision of 0.01 eV for the numerical integration in the LT step.

Reduction of Virtual Space. We also employed the reduction of the virtual space (RVS) approach to further reduce the computational costs.[25] In this work, virtual orbitals with orbital energies larger than 50 eV above the highest occupied molecular orbital (HOMO) were omitted in the correlation calculations. The RVS approach in combination with the CC2 family of methods has been successfully used to describe VEEs in several photobiological systems, including retinylidene proteins, green fluorescent protein, photoactive yellow protein, and lobster crustacyanine pigment.[51−57] For the monomeric Chl model, the omission of the higher-lying virtual orbitals introduces a small blueshift of 0.07 eV as compared to the corresponding full virtual space calculation at the LT-SOS-ADC(2)/def2-TZVP level (Table 2, Supporting Information).

EXCITATION ENERGIES

Comparison of Computational Methods. The results of the correlated *ab initio* calculations on the excited states of the monomeric Chl/BChl-L models are shown in Table 1. The calculations predict vertical excitation energies of 2.0−2.2 and 1.5−2.0 eV for the monomeric Chl-L and BChl-L models, respectively, which agree rather well with the absorption maxima at 1.87 and 1.60 eV in the experimental spectra measured in organic solvents.[58,59]

For the Chl-L model, the use of the LT-SOS approximation at the ADC(2)/def2-TZVP level introduces a small redshift of 0.04 eV in the excitation energy, while it reduces the computational time by approximately a factor of 4. Using the RVS approximation at the ADC(2)/def2-TZVP level introduces a small blueshift of 0.07 eV in the excitation energy, while the computational time is reduced by a factor of 5 as compared to a standard ADC(2) calculation. Using both the RVS and LT-SOS approximations at the ADC(2)/def2-TZVP level reduces the computational time from 31.7 to 3.6 h, speeding up the calculation by roughly a factor of 9. The errors introduced from the RVS and LT-SOS approximations cancel to some extent, leading to an overall error of 0.03 eV as compared to a standard ADC(2)/def2-TZVP calculation.

Table 1. Vertical Excitation Energy (VEE) Calculated at Different Levels of Theory Using def2-TZVP Basis Sets, as Well Required Computational Time for Chl/BChl Monomers Ligated by Histidines (-L)[a]

molecular system	method	VEE	CPU (h)
Chl-L	CC2	2.17	43.7
	+ RVS50	2.23	9.0
	LT-SOS-CC2	2.06	10.2
	+ RVS50	2.12	4.6
	ADC(2)	2.02	31.7
	+ RVS50	2.09	5.6
	LT-SOS-ADC(2)	1.98	7.5
	+RVS50	2.05	3.6
	B3LYP	2.14	9.9
BChl-L	CC2	1.97	30.8
	+ RVS50	2.02	6.4
	LT-SOS-CC2	1.79	9.3
	+ RVS50	1.85	4.4
	ADC(2)	1.46	21.2
	+ RVS50	1.54	4.4
	LT-SOS-ADC(2)	1.55	6.9
	+RVS50	1.62	3.2
	B3LYP	1.92	7.5

[a]The calculations were performed on Intel *Sandy Bridge* 2.6 GHz processors.

At the CC2/def2-TZVP level, the RVS approximation blueshifts the excitation energy by 0.06 eV, whereas the LT-SOS approximation redshifts the excitation energy by 0.11 eV. Again, using both the RVS and LT-SOS approximations speed up the CC2 calculations by almost an order of magnitude. The combined error of using both the RVS and the LT-SOS approximations at the CC2 level is 0.05 eV.

To study the size dependence of the employed methods, we performed calculations for the Chl, Chl-L, Chl_2, and Chl_2-L models at the ADC(2) and CC2 levels and their RVS/LT-SOS counterparts using def2-TZVP basis sets (Table 2, Supporting Information). The calculations suggest that the RVS50 error decreases from 0.07 eV (for Chl, Chl-L, and Chl_2) to 0.05 eV (for Chl_2-L) at the ADC(2) level. At the CC2 level, the RVS50 error remains constant at 0.06 eV for each model. The error of the LT-SOS approximation varies slightly more with the system size, which suggests that the error cancellation between the LT-SOS and RVS approximations might suffer with increasing system size. We also studied how the excitation energies depend on the employed structural models by using structures where all nonhydrogen atoms were kept fixed in their crystallographic positions. In comparison with the optimized models, the excitation energies shift by up to 0.3 eV, suggesting that structure optimization is central when calculating excitation energies (Table 3, Supporting Information).

For the BChl molecule, we obtain a surprisingly large difference of about 0.5 eV between the CC2 and ADC(2) methods. At the CC2 level, the lowest excitation energy for the monomeric BChl model without the histidine ligand is 1.99 eV,

DOI: 10.1021/acs.jctc.6b00237
J. Chem. Theory Comput. 2016, 12, 2644−2651

whereas the ADC(2) calculations yield 1.53 eV. The difference between the CC2 and ADC(2) energies is smaller when using the corresponding SOS model. The D_1 diagnostics for monomeric BChl is 0.076, suggesting that the molecule might to some extent suffer from multireference problems due to the near-degenerate orbitals of the symmetric BChl model. By breaking the symmetry of the BChl molecule with −CHO/−COOH substituents, the D_1 diagnostics decreases to 0.05−0.06 leading to a slight increase in the excitation energy to 1.62 eV, which agrees well with the maximum of the experimental absorption band at 1.60 eV.[59] The ADC(2) method, which has a hermitean Hamiltonian, was employed in this work since the charge densities of the ground and excited states can be obtained without solving the amplitude equations for the corresponding left states.

We also studied the performance of different basis sets at the LT-SOS-ADC(2) level, reported in Table 1 of the Supporting Information. For the monomeric and dimeric Chl models, the use of the def2-SVP basis sets leads to a small blueshift of 0.05 eV relative to the energies calculated using the aug-cc-pVDZ or the def2-TZVP basis sets.[31,60] For the tetrameric models, use of the def2-SVP basis sets instead of def2-TZVP blueshift the excitation energies by 0.06−0.12 eV for the P680, P700, and P870 models, while the orbital contributions of the excitations remain the same. The computational times required for calculating a single excited state for a Chl-L monomer (54 atoms), dimer (108 atoms), and tetramer (198 atoms) at the RVS-LT-SOS-ADC(2)/def2-SVP level are 1.3, 18.2, and 657.6 h, respectively. These results suggest that the smaller def2-SVP basis sets could be used in studies of very large systems. In this work, however, we have used the def2-TZVP basis sets for the excited state calculations, unless otherwise noted.

P680 Models of PSII. At the LT-SOS-RVS-ADC(2)/def2-TZVP level, we obtain a excitation energy of 2.05 eV for the Chl-L monomer, whereas for the dimeric model of P680, the calculated excitation energies are 2.04 and 2.06 eV, which corresponds to an excitonic splitting of 80 cm^{-1}. The obtained excitation energies are summarized in Table 2 and Figure 2, which also show the exciton densities, and suggest that the excitons are delocalized across the chlorohpylls of the central pair in the dimeric model.

Table 2. Vertical Excitation Energies (VEEs, in eV) of the Chl-L/BChl-L Clusters of PSII (P680), PSI (P700), and Bacterial RC (P870) Models Calculated at the RVS-LT-SOS-ADC2/def2-TZVP Level of theory

	P680 VEE	P700 VEE	P870 VEE
monomer	2.05	2.05	1.62
dimer	2.04	2.05	1.53
	2.06	2.10	1.62
tetramer	2.00	2.02	1.52
	2.01	2.04	1.56
	2.02	2.05	1.59
	2.04	2.07	1.62
exp.	1.82	1.77	1.42

For the tetrameric P680 model of PSII, we obtain excitation energies in the range of 2.00−2.04 eV for the lowest four states at the RVS-LT-SOS-ADC(2)/def2-TZVP level. The excitation energies are nearly degenerate, suggesting that the photoexcitation might lead to a multimeric excitation process, which is consistent with experimental observations.[61−63] The calculated excitation energies agree well with the experimental absorption maximum of 1.82 eV (680 nm) for P680, despite that the electrostatic effect of the protein environment is omitted. Although it is likely that error cancellation contributes to this good agreement, this could also suggest that the protein environment does not significantly shift the vertical excitation energies.

In the tetramer, the average excitation energy of the P_{D1}/P_{D2} pair (Figure 1A) is redshifted to 2.01 eV from the dimer value of 2.05 eV. We obtain an excitonic splitting of 80 cm^{-1} for the central P_{D1}/P_{D2} pair, corresponding to excitation energies of 2.00 and 2.02 eV for the individual monomers. For the Chl_{D1}/Chl_{D2} pair, we obtain an average excitation energy of 2.025 eV, which is redshifted by 0.025 eV relative to the monomer. This yields an excitonic splitting of 120 cm^{-1} between the outer chlorophylls, shifting their respective excitation energies to 2.01 and 2.04 eV. Our calculated excitonic splittings agree well with the experimental estimates of 50−150 cm^{-1}, despite the fact that the effect of the protein surroundings is not considered here explicitly.[1,61,64] The exciton density for these transitions, i.e., the difference in the charge density of the ground and excited states, shows that the excitons of the first and third excited states are delocalized over the P_{D1}/P_{D2} pair,[62,63] whereas the excitons of the second and fourth excited states reside on the monomeric $Chl_{D1/D2}$ pigments. However, thermal flucations may lead to reordering of these states due to their near degeneracy.[65]

P700 Models of PSI. For the tetrameric P700 model, we obtain excitation energies that range from 2.02 to 2.07 eV, yielding an average excitation energy of 2.045 eV for the four lowest states. The calculated excitonic splitting between the central P_A/P_B pair (Figure 1B) is 200 cm^{-1}, yielding excitation energies of 2.02 and 2.07 eV for P_A and P_B, respectively. Comparison to the dimeric model of P700, for which we obtain excitation energies of 2.05 and 2.10 eV and an excitonic splitting of 200 cm^{-1}, suggests that the interactions within the central tetramer unit might not affect the coupling between the central pair. For the outer A_A and A_B Chl molecules, we obtain excitation energies of 2.04 and 2.05 eV, corresponding to an excitonic splitting of 40 cm^{-1}. The calculated excitonic splittings agree well with the experimentally estimated values of 100−440 cm^{-1}.[1,66−69]

In contrast to P680, where our calculations suggest that the exciton is delocalized over both chlorophylls of the P_{D1}/P_{D2} pair, the excitons of the four lowest excited states of P700 reside on individual monomeric chlorophylls. We find that the exciton of the lowest excited state, with an energy of 2.02 eV, is located on one of the central P_A/P_B chlorophylls, whereas the excited state localized to the second P_A/P_B molecule is higher in energy due to the stronger excitonic coupling as compared to P680. These exciton densities are consistent with time-resolved experiments,[70] suggesting that relaxation of the excited P700 chromophore leads to a charge separation on the monomeric chlorophyll A_A/A_B instead of on the central P_A/P_B pair. The calculated excitation energies and exciton densities are reported in Table 2 and Figure 2, respectively.

P870 Models of RC. For the BChl-L monomer, we obtain an energy of 1.62 eV for the first excited state. The corresponding excitation energies of the two lowest states of the BChl-L dimer are 1.53 and 1.62 eV, yielding an average excitation energy of 1.575 eV and an excitonic splitting of 360 cm^{-1} between the two states. The calculations thus suggest that the interactions between the BChl units redshift the average

DOI: 10.1021/acs.jctc.6b00237
J. Chem. Theory Comput. 2016, 12, 2644−2651

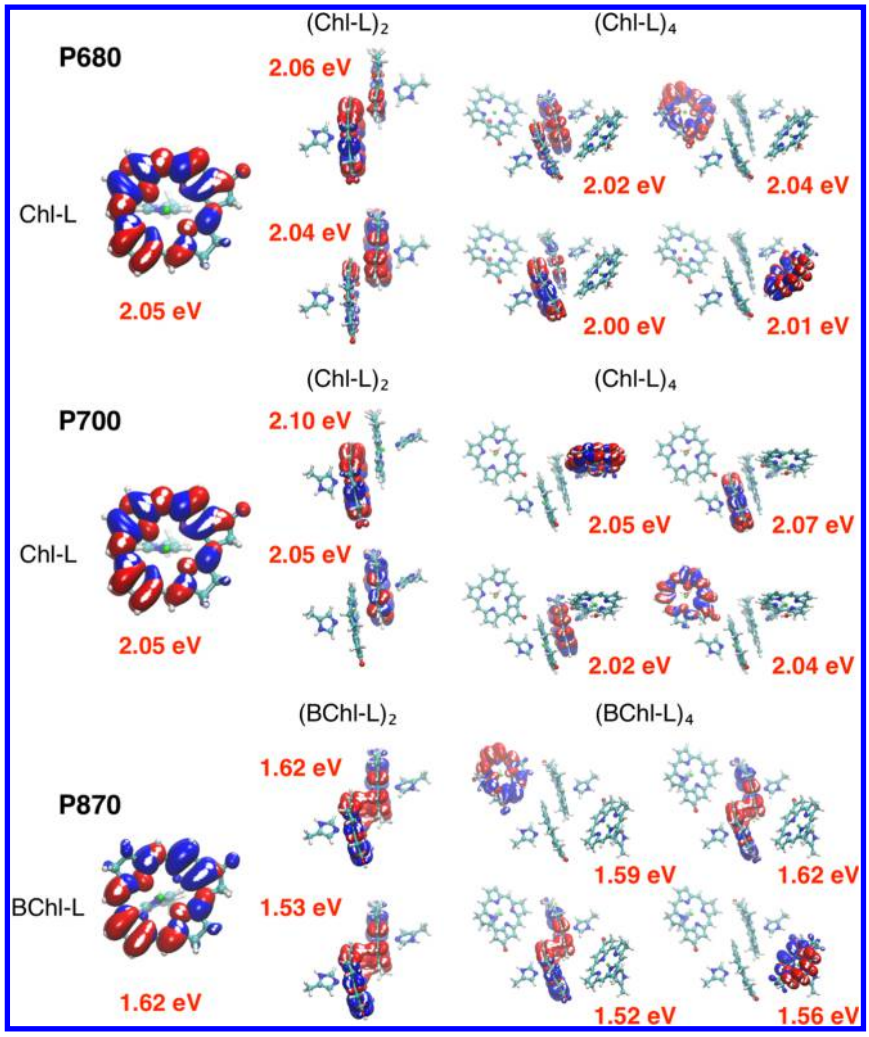


Figure 2. Exciton densities and vertical excitation energies of the studied P680, P700, and P870 models, obtained at the RVS-LT-SOS-ADC(2)/def2-TZVP level. The red and blue isocontour surfaces indicate increased and decreased electron density, respectively, for the excited states relative to the ground state.

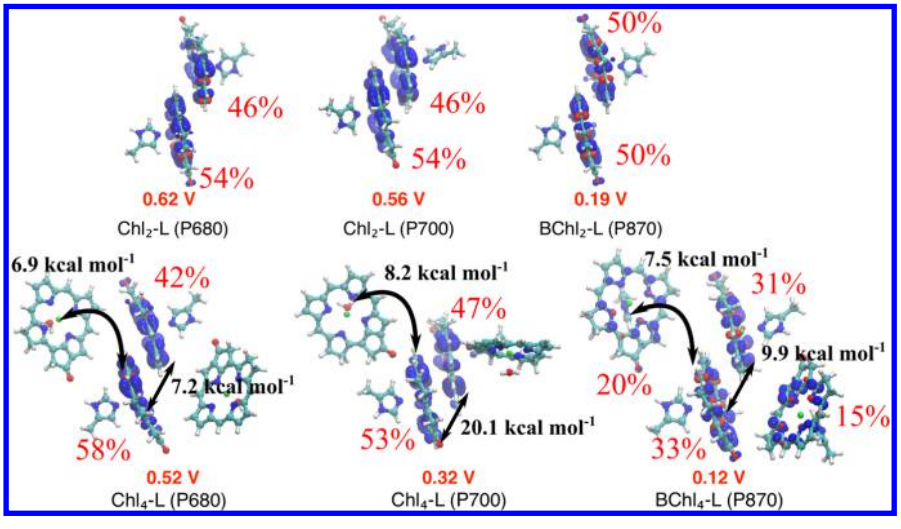


Figure 3. Oxidation potentials relative to the normal hydrogen electrode (NHE of 4.43 eV) for the Chl/BChl models calculated at the B3LYP-D3/def2-TZVP/COSMO level using $\epsilon_r = 4$. The first row shows the oxidation potentials of the dimeric models and the distribution of the spin density between the central chlorophylls. The second row shows the same data for the tetrameric Chl/BChl models of P680, P700, and P870. The interaction energies (in kcal mol^{-1}) between the chromophores are shown for the tetrameric models. The spin density distribution is plotted using an isocontour surface of $\pm 0.001e$ (in blue/red).

DOI: 10.1021/acs.jctc.6b00237
J. Chem. Theory Comput. 2016, 12, 2644−2651

excitation energy of the dimer by 0.045 eV relative to the monomer.

In the tetrameric P870 model, the calculated excitation energies are in the range of 1.52−1.62 eV, yielding an average excitation energy of 1.573 eV for the four lowest states. Thus, the outer BChl molecules ($BChl_L$ and $BChl_M$ in Figure 1C) blueshift the average excitation energy by 0.002 eV as compared to the dimeric model. We obtain a calculated excitonic splitting of ca. 400 cm^{-1} between the P_L and P_M pigments, yielding excitation energies of 1.52 and 1.62 eV for P_L and P_M, respectively. For the $BChl_L/BChl_M$ pigments, we obtain an excitonic splitting of 120 cm^{-1}, which corresponds to excitation energies of 1.56 and 1.59 eV for the individual $BChl_L$ and $BChl_M$ centers. We find that the excitons of the first and fourth excited states are delocalized over both molecules of the P_L/P_M pair (Figure 2). Our calculations thus suggest that the excitonic splitting of 400 cm^{-1} between the central P_L/P_M centers is significantly larger than for the central chlorophylls in our P680 and P700 models, with calculated values of 80 and 200 cm^{-1}, respectively. Despite the simplistic gas-phase pigment models employed here, the calculated excitonic splitting of the P870 model also agrees well with experimentally estimated values, which are in the range of 360−500 cm^{-1},[61,71] while values in the range of 500−1000 cm^{-1} have also previously been reported.[1,72]

Stacking Energies. The stacking interactions between the Chl/BChl pigments are known to influence, in addition to electronic couplings, their oxidation potentials (for review, see e.g., ref 1 and references therein). We therefore estimated the stacking energies within our P680, P700, and P870 pigment models, which we summarize in Figure 3. For the P680 model of PSII, we obtain a stacking energy of 7.2 kcal mol^{-1} between the central P_{D1}/P_{D2} pigments, which is similar in magnitude to the interaction energy of 6.9 kcal mol^{-1} that we obtain between the accessory pigments and the central P_{D1}/P_{D2} pair. The energies are very similar to the corresponding interaction energies of 9.9 and 7.5 kcal mol^{-1}, respectively, which we obtain for the P870 model of the bacterial RC. For the P700 model of PSI, however, we obtain an interaction energy of 20.1 kcal mol^{-1} between the central P_A/P_B chlorophylls. The significantly larger stacking energy for the P700 model can be a possible reason for the similar exciton densities in the PSII and RC models, as well as for the localization of the exciton to one of the P_A/P_B monomers in the PSI model. The difference in the chromophore stacking energies may also lead to shifts in the oxidation potentials, which may explain why P680 is a hot oxidant.[1]

OXIDATION POTENTIALS

For the P680 radical cation ($P680^{+/\bullet}$), we obtain an intrinsic electron affinity of 520 mV relative to the normal hydrogen electrode (NHE of 4.43 eV), which is 400 mV larger than for the P870 model and 200 mV larger than for the P700 model. The difference in electron affinities can partly be explained by the intrinsically higher oxidation potential of the Chl monomer relative to BChl.[1,17,19] At the DFT level, the difference in the electron affinity between the monomeric Chl and BChl models is 500 mV for a low-dielectric medium with a relative dielectric permittivity (ϵ_r) of 4. The electron affinity of the P680 model is 200 mV higher than for P700, even though the central pairs of the P680 and P700 models both consist of identical chlorophylls. For the dimeric models, the difference in the electron affinities of the P680 and P700 models is only 60 mV, suggesting that the neighboring Chl pigments strengthen the interaction between the central pair. The calculated electron affinities are summarized in Figure 3. We also studied how the electron affinities depend on the employed structural models and find that when estimating these properties from models where all nonhydrogen atoms were kept fixed in their crystallographic positions, the electron affinities differ by only 0.02−0.07 eV from the optimized models (Table 3, Supporting Information).

The radical of the cationic $P680^{+/\bullet}$ is asymmetrically localized (58%/42%) on the two monomers of the central P_{D1}/P_{D2} pair, as is also the exciton density, which supports experimental observations[73,74] as well as previous DFT calculations.[17,20] In contrast, we find that the spin density of the $P700^{+/\bullet}$ radical is more symmetrically (53%/47%) localized on the central P_A/P_B pair. For $P870^{+/\bullet}$, the radical distributes symmetrically over the special P_L/P_M pair. However, one-third of the spin density is delocalized to the neighboring $BChl_L/BChl_M$ pigments with an almost equal distribution of 15% and 20% of the spin density on $BChl_L$ and $BChl_M$, respectively.

DISCUSSION

The present ground state and excited state calculations at correlated *ab initio* and DFT levels reveal distinct differences and similarities between the type I and II photosynthetic chlorophyll clusters. The calculated excitonic couplings between the central pigment molecules vary between 80−400 cm^{-1} for the three studied tetrameric models. The exciton delocalizations across the central pair in the P680 and P870 models show interesting similarities. For the P700 model, the exciton is localized on one of the P_A/P_B pigments, although the P680 and P700 models consist of chemically identical Chl pigments. The findings correlate with the mechanistic similarities observed for the type II reaction centers of PSII and purple bacteria.[75]

The calculated excitonic coupling of 400 cm^{-1} in the P870 model is larger than the one we obtained for the P680 model. Nevertheless, we find that the stacking interaction energies of 7−9 kcal mol^{-1} between the central P_{D1}/P_{D2} (P_L/P_M) and the accessory Chl_{D1}/Chl_{D2} ($BChl_L/BChl_M$) pigments are similar in the two systems, which may partly explain why the exciton is delocalized across the central dimer in both systems.

The nearly degenerate excitation energies for the P_{D1}, P_{D2}, Chl_{D1}, and Chl_{D2} pigments of the P680 model can be expected to result in several alternative charge separation states, namely, Chl_{D1}^-/P_{D1}^+ and P_{D1}^+/P_{D2}^-, which also have been suggested based on time-resolved experiments probing the first few picoseconds after the photoexcitation process.[10]

In all photosynthetic systems, the relaxation of the excited state leads to photo-oxidation and formation of a charge separated cationic $P^{+/\bullet}$ state. Here, we find that the multimeric interactions in $P^{+/\bullet}$ have a large contribution to the oxidation potential, leading to a 200 mV shift between the P680 and P700 models, as well as a 500 mV shift relative to the P870 model.

On the basis of hybrid DFT calculations on a P680 dimer model using a relative dielectric permittivity (ϵ_r) of 2.2, Takahashi et al.[20] found that the cation radical is localized on the P_{D1}/P_{D2} pair in 54%/46% proportions, leading to a redox shift of 140 mV. Their results agree well with our estimate of 180 mV for the dimeric model when using an ϵ_r of 4, based on shifts calculated relative to monomeric chlorophylls with an electron affinity of 0.80 V. However, we find that the electron

DOI: 10.1021/acs.jctc.6b00237
J. Chem. Theory Comput. 2016, 12, 2644−2651

affinities are sensitive to the employed dielectric constants (Table 4 Supporting Information).

We also obtain a nearly symmetrically delocalized spin density for the P680 dimer model. In the calculations on the dimeric P680 and P700 models, we obtain a difference in the redox potential of only 60 mV, which increases to 200 mV for the tetrameric models. Thus, the calculations suggest that the stacking interaction with the neighboring Chl pigments is very important for the redox tuning.

The calculations show that the tetrameric P680 model has a 400 mV higher oxidation potential than the corresponding P870 model, which can partly be attributed to the intrinsic difference in the redox potential for monomeric Chl and BChl. Fajer et al.[19] found experimentally that the oxidation potential of Chl is 160 mV larger (more oxidizing) than for BChl, which correlates well with our computed difference of 220 mV for the monomeric Chl and BChl when using an ϵ_r of 4.

On the basis of DFT calculations on a dimeric model of P870, Yamasaki et al.[76] found that the cation is localized on the P_L side due to stacking of the pigments with a methyl substituent, which could further affect its oxidation potential. However, in the present calculations on the P870 models, we obtain a small shift of only 70 mV in the electron affinity between the dimeric and tetrameric P870 models, although the spin distribution drastically changes when also considering the accessory $BChl_L$ and $BChl_M$ pigments. The calculated spin-density is delocalized on all pigment molecules of the tetrameric P870 model.

In this work, the interactions between the central pair and the neighboring (B)Chl molecules are explicitly taken into account at the quantum mechanical level, whereas the electrostatic effect of the protein environment is modeled using an implicit solvent model. On the basis of hybrid quantum mechanics/classical mechanics (QM/MM) calculations, it has previously been suggested that the electrostatic field imposed by the protein environment shifts the positive charge ratio of P_{D1}/P_{D2} in P680 to about 80%/20%, whereas in the absence of the protein environment, the ratio was closer to 50%/50%.[77−79] Narzi et al.[79] recently found that the positive charge preferentially resides on P_{D1} in static calculations. However, they also found that dynamical effects introduce large fluctuations in the charge distribution, resulting in an average ratio of 56%/54% for the charge distribution between the pair. They also suggested that the exciton localization could be modulated in a similar manner.

SUMMARY AND CONCLUSIONS

In this work, we have studied the ground and excited state properties of photosynthetic chlorophyll and bacteriochlorophyll clusters of the P680, P700, and P870 pigments of type I and type II photosystems using large-scale correlated quantum chemical *ab initio* and density functional theory calculations. We address here for the first time multimerization effects using correlated *ab initio* theory, which is possible by using the algebraic diagrammatic construction through second-order (ADC(2)) method and the second-order approximate coupled-cluster (CC2) method in combination with the reduced virtual space (RVS) approach and the Laplace-transformed scaled-opposite-spin algorithm (LT-SOS) algorithm. The calculations show that the intrinsic organization of the Chl/BChl clusters leads to large differences in excitonic couplings and exciton localization properties. Moreover, we find that the stacking interaction between the chromophores plays a significant part in the redox tuning of the pigment clusters.

ASSOCIATED CONTENT

Supporting Information

The Supporting Information is available free of charge on the ACS Publications website at DOI: 10.1021/acs.jctc.6b00237.

Data of basis set convergence and benchmarking calculations for the RVS and LT-SOS approximations. (PDF)

Cartesian coordinates of the chlorophyll and bacteriochlorophyll models optimized at the B3LYP-D3/def2-SVP level. (ZIP)

AUTHOR INFORMATION

Corresponding Author

*E-mail: ville.kaila@ch.tum.de.

Author Contributions

C.-M. Suomivuori and N.O.C. Winter contributed equally.

Notes

The authors declare no competing financial interest.

ACKNOWLEDGMENTS

This work was carried out under the HPC-Europa2 project with the support of the European Commission − Capacities Area − Research Infrastructures. This research has also been supported by the Academy of Finland (AF) through projects 266227 and 275845, its Computational Science Research Programme (LASTU/258258), by AF and Deutscher Akademischer Austauschdienst (DAAD) within the AF-DAAD mobility project 287791, and by the Cluster of Excellence RESOLV (EXC 1069), funded by the Deutsche Forschungsgemeinschaft. Grants from COST Action CM1002, the Magnus Ehrnrooth Foundation, the Finnish Academy-German Academic Exchange Service, and the Jane and Aatos Erkko foundation are greatly appreciated. The Finnish IT Center for Science (CSC) and the Leibniz Rechenzentrum (LRZ) are acknowledged for computer time.

REFERENCES

(1) Cardona, T.; Sedoud, A.; Cox, N.; Rutherford, A. W. *Biochim. Biophys. Acta, Bioenerg.* **2012**, *1817*, 26−43.

(2) Tommos, C.; Babcock, G. T. *Biochim. Biophys. Acta, Bioenerg.* **2000**, *1458*, 199−219.

(3) Wikström, M.; Sharma, V.; Kaila, V. R. I.; Hosler, J. P.; Hummer, G. *Chem. Rev.* **2015**, *115*, 2196−2221.

(4) Umena, Y.; Kawakami, K.; Shen, J.-R.; Kamiya, N. *Nature* **2011**, *473*, 55−60.

(5) Jordan, P.; Fromme, P.; Witt, H. T.; Klukas, O.; Saenger, W.; Krauß, N. *Nature* **2001**, *411*, 909−917.

(6) Fujii, R.; Adachi, S.; Roszak, A. W.; Gardiner, A. T.; Cogdell, R. J.; Isaacs, N. W.; Koshihara, S.; Hashimoto, H. Structure of the carotenoid bound to the reaction centre from rhodobacter sphaeroides 2.4.1 revealed by time-resolved X-ray crystallography (unpublished).

(7) Hashimoto, H.; Sugai, Y.; Uragami, C.; Gardiner, A. T.; Cogdell, R. J. *J. Photochem. Photobiol., C* **2015**, *25*, 46−70.

(8) Kaufmann, K.; Dutton, P.; Netzel, T.; Leigh, J.; Rentzepis, P. *Science* **1975**, *188*, 1301−1304.

(9) Rockley, M. G.; Windsor, M. W.; Cogdell, R. J.; Parson, W. W. *Proc. Natl. Acad. Sci. U. S. A.* **1975**, *72*, 2251−2255.

(10) Dekker, J. P.; Van Grondelle, R. *Photosynth. Res.* **2000**, *63*, 195−208.

(11) Rappaport, F.; Diner, B. A. *Coord. Chem. Rev.* **2008**, *252*, 259−272.

DOI: 10.1021/acs.jctc.6b00237
J. Chem. Theory Comput. 2016, 12, 2644−2651

(12) Rappaport, F.; Guergova-Kuras, M.; Nixon, P. J.; Diner, B. A.; Lavergne, J. *Biochemistry* **2002**, *41*, 8518−8527.
(13) Williams, J. C.; Alden, R. G.; Murchison, H. A.; Peloquin, J. M.; Woodbury, N. W.; Allen, J. P. *Biochemistry* **1992**, *31*, 11029−11037.
(14) Brettel, K. *Biochim. Biophys. Acta, Bioenerg.* **1997**, *1318*, 322−373.
(15) Rutherford, A. W.; Nitschke, W. In *Origin and Evolution of Biological Energy Conversion*; Baltscheffsky, H., Ed.; VCH: New York, 1996; pp 143−175.
(16) Rutherford, A.; Faller, P. *Philos. Trans. R. Soc., B* **2003**, *358*, 245−253.
(17) Ishikita, H.; Saenger, W.; Biesiadka, J.; Loll, B.; Knapp, E.-W. *Proc. Natl. Acad. Sci. U. S. A.* **2006**, *103*, 9855−9860.
(18) Ishikita, H.; Loll, B.; Biesiadka, J.; Saenger, W.; Knapp, E.-W. *Biochemistry* **2005**, *44*, 4118−4124.
(19) Fajer, J.; Brune, D.; Davis, M.; Forman, A.; Spaulding, L. *Proc. Natl. Acad. Sci. U. S. A.* **1975**, *72*, 4956−4960.
(20) Takahashi, R.; Hasegawa, K.; Noguchi, T. *Biochemistry* **2008**, *47*, 6289−6291.
(21) Jung, Y.; Lochan, R. C.; Dutoi, A. D.; Head-Gordon, M. *J. Chem. Phys.* **2004**, *121*, 9793−9802.
(22) Rhee, Y. M.; Head-Gordon, M. *J. Phys. Chem. A* **2007**, *111*, 5314−5326.
(23) Winter, N. O. C.; Hättig, C. *J. Chem. Phys.* **2011**, *134*, 184101.
(24) Winter, N. O. C.; Hättig, C. *Chem. Phys.* **2012**, *401*, 217−227.
(25) Send, R.; Kaila, V. R. I.; Sundholm, D. *J. Chem. Phys.* **2011**, *134*, 214114.
(26) Sundholm, D. *Chem. Phys. Lett.* **1999**, *302*, 480−484.
(27) Becke, A. D. *J. Chem. Phys.* **1993**, *98*, 5648−5652.
(28) Lee, C.; Yang, W.; Parr, R. G. *Phys. Rev. B: Condens. Matter Mater. Phys.* **1988**, *37*, 785−789.
(29) Grimme, S.; Antony, J.; Ehrlich, S.; Krieg, H. *J. Chem. Phys.* **2010**, *132*, 154104.
(30) Schäfer, A.; Horn, H.; Ahlrichs, R. *J. Chem. Phys.* **1992**, *97*, 2571−2577.
(31) Weigend, F.; Ahlrichs, R. *Phys. Chem. Chem. Phys.* **2005**, *7*, 3297−3305.
(32) Klamt, A.; Schüürmann, G. *J. Chem. Soc., Perkin Trans. 2* **1993**, 799−805.
(33) Schäfer, A.; Klamt, A.; Sattel, D.; Lohrenz, J. C. W.; Eckert, F. *Phys. Chem. Chem. Phys.* **2000**, *2*, 2187−2193.
(34) Schirmer, J. *Phys. Rev. A: At., Mol., Opt. Phys.* **1982**, *26*, 2395−2416.
(35) Weigend, F.; Häser, M. *Theor. Chem. Acc.* **1997**, *97*, 331−340.
(36) Hättig, C.; Weigend, F. *J. Chem. Phys.* **2000**, *113*, 5154−5161.
(37) Köhn, A.; Hättig, C. *J. Chem. Phys.* **2003**, *119*, 5021−5036.
(38) Hättig, C. *Adv. Quantum Chem.* **2005**, *50*, 37−60.
(39) Ahlrichs, R.; Bär, M.; Häser, M.; Horn, H.; Kölmel, C. *Chem. Phys. Lett.* **1989**, *162*, 165−169. Current version: see http://www.turbomole.com.
(40) Furche, F.; Ahlrichs, R.; Hättig, C.; Klopper, W.; Sierka, M.; Weigend, F. *WIREs Comput. Mol. Sci.* **2014**, *4*, 91−100.
(41) Christiansen, O.; Koch, H.; Jørgensen, P. *Chem. Phys. Lett.* **1995**, *243*, 409−418.
(42) Head-Gordon, M.; Rico, R. J.; Oumi, M.; Lee, T. J. *Chem. Phys. Lett.* **1994**, *219*, 21−29.
(43) Hättig, C. In *Computational Nanoscience: Do It Yourself!*; Grotendorst, J., Blugel, S., Marx, D., Eds.; NIC Series; John von Neumann Institute for Computing: Jülich, 2006; Vol. *31*; pp 245−278.
(44) Winter, N. O. C.; Graf, N. K.; Leutwyler, S.; Hättig, C. *Phys. Chem. Chem. Phys.* **2013**, *15*, 6623−6630.
(45) Schreiber, M.; Silva-Junior, M. R.; Sauer, S. P.; Thiel, W. *J. Chem. Phys.* **2008**, *128*, 134110.
(46) Koch, H.; Christiansen, O.; Jørgensen, P.; Olsen, J. *Chem. Phys. Lett.* **1995**, *244*, 75−82.
(47) Tuna, D.; Lefrancois, D.; Wolanski, Ł; Gozem, S.; Schapiro, I.; Andruniów, T.; Dreuw, A.; Olivucci, M. *J. Chem. Theory Comput.* **2015**, *11*, 5758−5781.
(48) Hättig, C.; Köhn, A. *J. Chem. Phys.* **2002**, *117*, 6939−6951.
(49) Hättig, C. *J. Chem. Phys.* **2003**, *118*, 7751−7761.
(50) Rhee, Y. M.; Casanova, D.; Head-Gordon, M. *J. Phys. Chem. A* **2009**, *113*, 10564−10576.
(51) Kaila, V. R. I.; Send, R.; Sundholm, D. *J. Phys. Chem. B* **2012**, *116*, 2249−2258.
(52) Zhou, X.; Sundholm, D.; Wesołowski, T. A.; Kaila, V. R. I. *J. Am. Chem. Soc.* **2014**, *136*, 2723−2726.
(53) Send, R.; Suomivuori, C.-M.; Kaila, V. R. I.; Sundholm, D. *J. Phys. Chem. B* **2015**, *119*, 2933−2945.
(54) Kaila, V. R. I.; Send, R.; Sundholm, D. *Phys. Chem. Chem. Phys.* **2013**, *15*, 4491−4495.
(55) Gamiz-Hernandez, A. P.; Angelova, I. N.; Send, R.; Sundholm, D.; Kaila, V. R. I. *Angew. Chem., Int. Ed.* **2015**, *54*, 11564−11566.
(56) Gamiz-Hernandez, A. P.; Kaila, V. R. I. *Phys. Chem. Chem. Phys.* **2016**, *18*, 2802−2809.
(57) Suomivuori, C.-M.; Lang, L.; Gamiz-Hernandez, A. P.; Sundholm, D.; Kaila, V. R. I. *Chem. - Eur. J.* **2016**, DOI: 10.1002/chem.201505126.
(58) Björn, L. O.; Papageorgiou, R. E.; Blankenship, G. C.; Govindjee. *Photosynth. Res.* **2009**, *99*, 85−98.
(59) Linnanto, J.; Korppi-Tommola, J. *J. Phys. Chem. A* **2001**, *105*, 3855−3866.
(60) Dunning, T. H., Jr. *J. Chem. Phys.* **1989**, *90*, 1007−1023.
(61) Durrant, J. R.; Klug, D. R.; Kwa, S. L.; Van Grondelle, R.; Porter, G.; Dekker, J. P. *Proc. Natl. Acad. Sci. U. S. A.* **1995**, *92*, 4798−4802.
(62) Raszewski, G.; Diner, B. A.; Schlodder, E.; Renger, T. *Biophys. J.* **2008**, *95*, 105−119.
(63) Cox, N.; Hughes, J. L.; Steffen, R.; Smith, P. J.; Rutherford, A. W.; Pace, R. J.; Krausz, E. *J. Phys. Chem. B* **2009**, *113*, 12364−12374.
(64) Renger, T.; Schlodder, E. *ChemPhysChem* **2010**, *11*, 1141−1153.
(65) Novoderezhkin, V. I.; Romero, E.; van Grondelle, R. *Phys. Chem. Chem. Phys.* **2015**, *17*, 30828−30841.
(66) Beddard, G. S. *J. Phys. Chem. B* **1998**, *102*, 10966−10973.
(67) Adolphs, J.; Müh, F.; Madjet, M. E.; Schmidt am Busch, M.; Renger, T. *J. Am. Chem. Soc.* **2010**, *132*, 3331−3343.
(68) Schlodder, E.; Lendzian, F.; Meyer, J.; Cetin, M.; Brecht, M.; Renger, T.; Karapetyan, N. V. *J. Am. Chem. Soc.* **2014**, *136*, 3904−3918.
(69) Schlodder, E.; Shubin, V. V.; El-Mohsnawy, E.; Roegner, M.; Karapetyan, N. V. *Biochim. Biophys. Acta, Bioenerg.* **2007**, *1767*, 732−741.
(70) Di Donato, M.; Stahl, A.; van Stokkum, I.; van Grondelle, R.; Groot, M. *Biochemistry* **2011**, *50*, 480−490.
(71) Timpmann, K.; Trinkunas, G.; Olsen, J. D.; Hunter, C. N.; Freiberg, A. *Chem. Phys. Lett.* **2004**, *398*, 384−388.
(72) Woodbury, N. W.; Allen, J. P. The Pathway, Kinetics and Thermodynamics of Electron Transfer in Wild Type and Mutant Reaction Centers of Purple Nonsulfur Bacteria. In *Anoxygenic Photosynthetic Bacteria*; Blankenship, R. E., Madigan, M. T., Bauer, C. E., Ed.; Kluwer Academic Publishers: The Netherlands, 1995; pp 527−557.
(73) Groot, M. L.; Pawlowicz, N. P.; van Wilderen, L. J.; Breton, J.; van Stokkum, I. H.; van Grondelle, R. *Proc. Natl. Acad. Sci. U. S. A.* **2005**, *102*, 13087−13092.
(74) Holzwarth, A.; Müller, M.; Reus, M.; Nowaczyk, M.; Sander, J.; Rögner, M. *Proc. Natl. Acad. Sci. U. S. A.* **2006**, *103*, 6895−6900.
(75) Diner, B. A.; Rappaport, F. *Annu. Rev. Plant Biol.* **2002**, *53*, 551−580.
(76) Yamasaki, H.; Nakamura, H.; Takano, Y. *Chem. Phys. Lett.* **2007**, *447*, 324−329.
(77) Saito, K.; Ishida, T.; Sugiura, M.; Kawakami, K.; Umena, Y.; Kamiya, N.; Shen, J.-R.; Ishikita, H. *J. Am. Chem. Soc.* **2011**, *133*, 14379−14388.
(78) Saito, K.; Umena, Y.; Kawakami, K.; Shen, J.-R.; Kamiya, N.; Ishikita, H. *Biochemistry* **2012**, *51*, 4290−4299.
(79) Narzi, D.; Bovi, D.; De Gaetano, P.; Guidoni, L. *J. Am. Chem. Soc.* **2016**, *138*, 257−264.

DOI: 10.1021/acs.jctc.6b00237
J. Chem. Theory Comput. 2016, 12, 2644−2651